(12) INTERNATIONAL APPLICATION PUBLISHED UNDER THE PATENT COOPERATION TREATY (PCT)

(19) World Intellectual Property Organization
International Bureau

(43) International Publication Date
13 March 2003 (13.03.2003)

PCT

(10) International Publication Number
WO 03/021524 A1

(51) International Patent Classification[7]: G06K 9/00

(21) International Application Number: PCT/US02/28070

(22) International Filing Date:
5 September 2002 (05.09.2002)

(25) Filing Language: English

(26) Publication Language: English

(30) Priority Data:
60/316,965 5 September 2001 (05.09.2001) US
10/233,562 4 September 2002 (04.09.2002) US

(71) Applicant: VIRTUALSCOPICS, LLC [US/US]; 160 Office Parkway, Rochester, NY 14534 (US).

(72) Inventors: TOTTERMAN, Saara Marjatta Sofia; 195 Dunrovin Lane, Rochester, NY 14618 (US). TAMEZ-PENA, Jose; 111 Lac de Ville Boulevard, Apt. 301, Rochester, NY 14620 (US). ASHTON, Edward; 87 Granger Circle, Webster, NY 14580 (US). PARKER, Kevin; 166 Superior Road, Rochester, NY 14625 (US).

(74) Agents: GREENBAUM, Michael, C. et al.; Blank Rome Comisky & McCauley LLP, 900 17th Street, NW, Suite 1000, Washington, DC 20006 (US).

(81) Designated States *(national)*: AE, AG, AL, AM, AT, AU, AZ, BA, BB, BG, BR, BY, BZ, CA, CH, CN, CO, CR, CU, CZ, DE, DK, DM, DZ, EC, EE, ES, FI, GB, GD, GE, GH, GM, HR, HU, ID, IL, IN, IS, JP, KE, KG, KP, KR, KZ, LC, LK, LR, LS, LT, LU, LV, MA, MD, MG, MK, MN, MW, MX, MZ, NO, NZ, OM, PH, PL, PT, RO, RU, SD, SE, SG, SI, SK, SL, TJ, TM, TN, TR, TT, TZ, UA, UG, UZ, VC, VN, YU, ZA, ZM, ZW.

(84) Designated States *(regional)*: ARIPO patent (GH, GM, KE, LS, MW, MZ, SD, SL, SZ, TZ, UG, ZM, ZW), Eurasian patent (AM, AZ, BY, KG, KZ, MD, RU, TJ, TM), European patent (AT, BE, BG, CH, CY, CZ, DE, DK, EE, ES, FI, FR, GB, GR, IE, IT, LU, MC, NL, PT, SE, SK, TR), OAPI patent (BF, BJ, CF, CG, CI, CM, GA, GN, GQ, GW, ML, MR, NE, SN, TD, TG).

[Continued on next page]

(54) Title: SYSTEM AND METHOD FOR QUANTITATIVE ASSESSMENT OF NEUROLOGICAL DISEASES AND THE CHANGE OVER TIME OF NEUROLOGICAL DISEASES

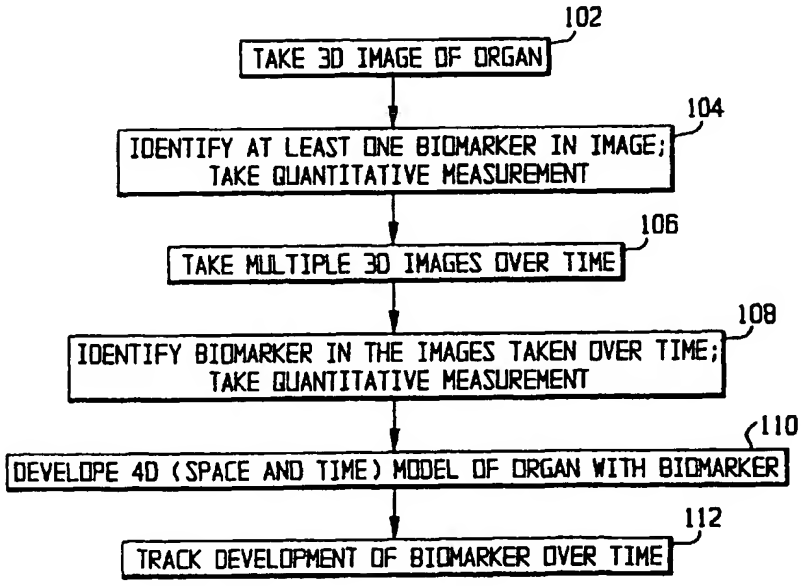

(57) Abstract: In a human or animal brain or other nerve tissue, specific objects or conditions, such as brain lesions and plaques, serve as indicators, or biomarkers, of neurological disease. In a three-dimensional image of the region of interest (102), the biomarkers are identified and quantified (104). Multiple three-dimensional images can be taken over time, in which the biomarkers can be tracked over time (106 and 108). Statistical segmentation techniques are used to identify the biomarker in a first image and to carry the identification over to the remaining images.

WO 03/021524 A1

Published:
— *with international search report*

For two-letter codes and other abbreviations, refer to the "Guidance Notes on Codes and Abbreviations" appearing at the beginning of each regular issue of the PCT Gazette.

SYSTEM AND METHOD FOR QUANTITATIVE ASSESSMENT OF NEUROLOGICAL DISEASES AND THE CHANGE OVER TIME OF NEUROLOGICAL DISEASES

Reference to Related Applications

The present application claims the benefit of U.S. Provisional Application No. 60/316,965, filed September 5, 2001, whose disclosure is hereby incorporated by reference in its entirety into the present disclosure.

Field of the Invention

The present invention is directed to a system and method for quantifying neurological diseases and their change over time and is more particularly directed to such a system and method which use biomarkers related to the nervous system, or neuromarkers.

Description of Related Art

Diseases of the nervous system, such as multiple sclerosis, Alzheimer's disease, and other degenerative conditions, afflict a significant percent of the population. In assessing those conditions, and in tracking their change over time, including improvements due to new therapies, it is necessary to have quantitative information. Subjective and/or difficult to quantify measures of functional degeneration have been used in the past. Such measures lack sensitivity, and are typically useful only in the latter stages of disease. Less subjective measures can be obtained from measurements of conventional 2D images on computed tomography (CT) and magnetic resonance (MRI) images, but those are traditionally assessed through manual tracings, or by caliper measurements of the image. Examples of measurements that are taken from MRI examinations of multiple sclerosis patients include: lesion volume (T2, PDW, FLAIR, Gd-enhancing), whole brain volume,

volume of a particular part of the brain, and intra-cranial CSF volume. Typical measurements for assessment of Alzheimer's disease include: volume of the whole gray matter, white matter, CSF space, anterior and medial temporal lobe, hippocampus, and entorhinal cortex.

Some references for the prior work include:

Rovaris M, Inglese M, van Shijndel RA, et al. "Sensitivity and reproducibility of volume change measurements of different brain portions on magnetic resonance imaging in patients with multiple sclerosis." *Journal of Neurology*. 247(12):960-5, 2000.

Rovaris M, Bastianello S, Capra R, et al. "Correlation between enhancing lesion number and volume on standard and triple dose gadolinium-enhanced brain MRI scans from patients with multiple sclerosis." *Magnetic Resonance Imaging*. 17(7):985-8, 1999.

Dastidar P, Hainonen T, Lehtimaki T, et al. "Volumes of atrophy and plaques correlated with neurological disability in secondary progressive multiple sclerosis." *Journal of the Neurological Sciences*. 165(1):36-45, 1999.

Guttmann CR, Kikinis R, Anderson MC, et al. "Quantitative follow-up of patients with multiple sclerosis using MRI: reproducibility." *Journal of Magnetic Resonance Imaging*. 9(4):509-19, 1999.

Heinonen T, Dastidar P, Eskola H, et al. "Applicability of semi-automatic segmentation for volumetric analysis of brain lesions." *Journal of Medical Engineering & Technology*. 22(4):173-8, 1998.

Jack CR Jr, Peterson RC, O'Brien PC, et al. "MR-based hippocampal volumetry in the diagnosis of Alzheimer's disease." *Neurology*. 42(1)183-8, 1992.

Xu Y, Jack CR Jr, O'Brien PC, et al. "Usefulness of MRI measures of entorhinal cortex versus hippocampus in AD." *Neurology*. 54(9):1760-7, 2000.

Brunetti A, Postiglione A, Tedeschi E, et al. "Measurement of global brain atrophy in Alzheimer's disease with unsupervised segmentation of spin-echo MRI studies." *Journal of Magnetic Resonance Imaging*. 11(3):260-6, 2000.

Mizuno K, Wakai M, Takeda A, et al. "Medial temporal atrophy and memory impairment in early stage of Alzheimer's disease: an MRI volumetric and memory assessment study." *Journal of Neurological Sciences* 173(1):18-24, 2000.

Juottonen K, Laasko MP, Insausti R, et al. "Volumes of the entorhinal and perirhinal cortices in Alzheimer's disease." *Neurobiology of Aging*. 19(1):15-22, 1998.

Those measurements require manual or semi-manual systems that require a user to identify the structure of interest and to trace boundaries or areas, or to initialize an active contour.

The prior art is capable of assessing gross abnormalities or gross changes over time. However, the conventional measurements are not well suited to assessing and quantifying subtle abnormalities, or subtle changes, and are incapable of describing complex topology or shape in an accurate manner. Furthermore, manual and semi-manual measurements from raw images suffer from a high inter- and intra-observer variability. Also, manual and semi-manual measurements tend to produce ragged and irregular boundaries in 3D when the tracings are based on a sequence of 2D images.

Summary of the Invention

It will be apparent from the above that a need exists in the art to identify important structures or substructures, their normalities and abnormalities, and their specific topological and morphological characteristics. It is therefore a primary object of the invention to provide a more accurate quantification of neurological tissue structures. It is another object of the invention to provide a more accurate quantification of changes in time of those tissue structures. It is a further object of the invention to address the needs noted above.

To achieve the above and other objects, the present invention is directed to an identification of important structures or substructures, their normalities and abnormalities, and to an identification of their specific topological, morphological, radiological and pharmacokinetic characteristics, which are sensitive indicators of neurological disease and the state of pathology. The abnormality and normality of structures, along with their topological and morphological characteristics and radiological and pharmacokinetic parameters are called biomarkers, or are alternatively called neuromarkers if they are specific to neurology. Specific measurements of the biomarkers serve as the quantitative assessment of neurological disease.

The inventors have discovered that the following new biomarkers are sensitive indicators of neurological disease in humans and in animals:

- The shape, topology, and morphology of brain lesions;
- The shape, topology, and morphology of brain plaques;
- The shape, topology, and morphology of brain ischemia;
- The shape, topology, and morphology of brain tumors;
- The spatial frequency distribution of the sulci and gyri;

- The compactness (a measure of surface to volume ratio) of gray matter and white matter;
- Whole brain characteristics;
- Gray matter characteristics;
- White matter characteristics;
- Cerebral spinal fluid characteristics;
- Hippocampus characteristics;
- brain sub-structure characteristics;
- The ratio of cerebral spinal fluid volume to gray matter and white matter volume; and
- The number and volume of brain lesions.

A preferred method for extracting the biomarkers is with statistical based reasoning as defined in *Parker et al* (US Patent 6,169,817), whose disclosure is hereby incorporated by reference in its entirety into the present disclosure. A preferred method for quantifying shape and topology is with the morphological and topological formulas as defined by the following references:

Curvature Analysis: Peet, F.G., Sahota, T.S. "Surface Curvature as a Measure of Image Texture" *IEEE Transactions on Pattern Analysis and Machine Intelligence 1985* Vol PAMI-7 G:734-738;

Struik, D.J., *Lectures on Classical Differential Geometry*, 2nd ed., Dover, 1988.

Shape and Topological Descriptors: Duda, R.O, Hart, P.E., *Pattern Classification and Scene Analysis*, Wiley & Sons, 1973.

Jain, A.K, *Fundamentals of Digital Image Processing*, Prentice Hall, 1989.

Spherical Harmonics: Matheny, A., Goldgof, D. "The Use of Three and Four Dimensional Surface Harmonics for Nonrigid Shape Recovery and Representation," *IEEE Transactions on Pattern Analysis and Machine Intelligence 1995*, 17: 967-981; Chen, C.W, Huang, T.S., Arrot, M. "Modeling, Analysis, and Visualization of Left Ventricle Shape and Motion by Hierarchical Decomposition," *IEEE Transactions on Pattern Analysis and Machine Intelligence 1994*, 342-356.

Those morphological and topological measurements have not in the past been applied to those neurological biomarkers.

The quantitative assessment of the new biomarkers listed above provides an objective measurement of the state of the nervous system, particularly in the progression of neurological disease. It is also very useful to obtain accurate measurements of those biomarkers over time, particularly to judge the degree of response to a new therapy, or to assess the trends with increasing age. Manual and semi-manual tracings of conventional biomarkers (such as the simple volume of the brain) have a high inherent variability, so that as successive scans are traced, the variability can hide subtle trends. That means that only gross changes, sometimes over very long time periods, can be verified using conventional methods. The inventors have discovered that extracting the biomarker using statistical tests and treating the biomarker over time as a 4D object, with an automatic passing of boundaries from one time interval to the next, can provide a highly accurate and reproducible segmentation from which trends over time can be detected. That preferred approach is defined in the above-cited *Parker et al* patent. Thus, the combination of selected biomarkers that themselves capture subtle pathologies, with a 4D approach to increase accuracy and reliability over time, creates sensitivity that has not been previously obtainable.

Brief Description of the Drawings

A preferred embodiment of the present invention will be set forth in detail with reference to the drawings, in which:

Fig. 1 shows a flow chart of an overview of the process of the preferred embodiment;

Fig. 2 shows a flow chart of a segmentation process used in the process of Fig. 1;

Fig. 3 shows a process of tracking a segmented image in multiple images taken over time; and

Fig. 4 shows a block diagram of a system on which the process of Figs. 1-3 can be implemented.

Detailed Description of the Preferred Embodiment

A preferred embodiment of the present invention will now be set forth with reference to the drawings.

Fig. 1 shows an overview of the process of identifying biomarkers and their trends over time. In step 102, a three-dimensional image of the region of interest is taken. In step 104, at least one biomarker is identified in the image; the technique for doing so will be explained with reference to Fig. 2. Also in step 104, at least one quantitative measurement is made of the biomarker. In step 106, multiple three-dimensional images of the same region of the region of interest are taken over time. In some cases, step 106 may be completed before step 104; the order of those two steps is a matter of convenience. In step 108, the same biomarker or biomarkers and their quantitative measurements are identified in the images taken over time; the technique for doing so will be explained with reference to Fig. 3. The identification of the biomarkers in the multiple image allows the development in step 110 of a model of the region of interest in four dimensions, namely, three dimensions of space and one of time. From that model, the development of the biomarker or biomarkers can be tracked over time in step 112.

The preferred method for extracting the biomarkers is with statistical based reasoning as defined in *Parker et al* (US Patent 6,169,817), whose disclosure is hereby incorporated by reference in its entirety into the present disclosure. From raw image data obtained through magnetic resonance imaging or the like, an object is reconstructed and visualized in four dimensions (both space and time) by first dividing the first image in the sequence of images into regions through statistical estimation of the mean value and variance of the image data and joining of picture elements (voxels) that are sufficiently similar and then extrapolating the regions to the

remainder of the images by using known motion characteristics of components of the image (e.g., spring constants of muscles and tendons) to estimate the rigid and deformational motion of each region from image to image. The object and its regions can be rendered and interacted with in a four-dimensional (4D) virtual reality environment, the four dimensions being three spatial dimensions and time.

The segmentation will be explained with reference to Fig. 2. First, at step 201, the images in the sequence are taken, as by an MRI. Raw image data are thus obtained. Then, at step 203, the raw data of the first image in the sequence are input into a computing device. Next, for each voxel, the local mean value and region variance of the image data are estimated at step 205. The connectivity among the voxels is estimated at step 207 by a comparison of the mean values and variances estimated at step 205 to form regions. Once the connectivity is estimated, it is determined which regions need to be split, and those regions are split, at step 209. The accuracy of those regions can be improved still more through the segmentation relaxation of step 211. Then, it is determined which regions need to be merged, and those regions are merged, at step 213. Again, segmentation relaxation is performed, at step 215. Thus, the raw image data are converted into a segmented image, which is the end result at step 217. Further details of any of those processes can be found in the above-cited *Parker et al* patent.

The creation of a 4D model (in three dimensions of space and one of time) will be described with reference to Fig. 3. A motion tracking and estimation algorithm provides the information needed to pass the segmented image from one frame to another once the first image in the sequence and the completely segmented image derived therefrom as described above have been input at step 301. The presence of both the rigid and non-rigid components should ideally be taken into

account in the estimation of the 3D motion. According to the present invention, the motion vector of each voxel is estimated after the registration of selected feature points in the image.

To take into consideration the movement of the many structures present in the region of interest, the approach of the present invention takes into account the local deformations of soft tissues by using *a priori* knowledge of the material properties of the different structures found in the image segmentation. Such knowledge is input in an appropriate database form at step 303. Also, different strategies can be applied to the motion of the rigid structures and to that of the soft tissues. Once the selected points have been registered, the motion vector of every voxel in the image is computed by interpolating the motion vectors of the selected points. Once the motion vector of each voxel has been estimated, the segmentation of the next image in the sequence is just the propagation of the segmentation of the former image. That technique is repeated until every image in the sequence has been analyzed.

The definition of time and the order of sequencing can be reversed for the purpose of analysis. For example, brain lesions in the final image may be used as a starting point, with time reversal processing. Similarly, the midpoint of a time series may be used as a convenient starting point, with analysis proceeding in both forward and reverse directions.

Finite-element models (FEM) are known for the analysis of images and for time-evolution analysis. The present invention follows a similar approach and recovers the point correspondence by minimizing the total energy of a mesh of masses and springs that models the physical properties of the anatomy. In the present invention, the mesh is not constrained by a single structure in the image, but instead is free to model the whole volumetric image, in which topological properties are

supplied by the first segmented image and the physical properties are supplied by the *a priori* properties and the first segmented image. The motion estimation approach is an FEM-based point correspondence recovery algorithm between two consecutive images in the sequence. Each node in the mesh is an automatically selected feature point of the image sought to be tracked, and the spring stiffness is computed from the first segmented image and *a priori* knowledge of the human anatomy and typical biomechanical properties for the tissues in the region of interest.

Many deformable models assume that a vector force field that drives spring-attached point masses can be extracted from the image. Most such models use that approach to build semi-automatic feature extraction algorithms. The present invention employs a similar approach and assumes that the image sampled at $t = n$ is a set of three dynamic scalar fields:

$\Phi(\mathbf{x},t) = \{g_n(\mathbf{x}), |\nabla g_n(\mathbf{x})|, \nabla^2 g_n(\mathbf{x})\}$,

namely, the gray-scale image value, the magnitude of the gradient of the image value, and the Laplacian of the image value. Accordingly, a change in $\Phi(\mathbf{x}, t)$ causes a quadratic change in the scalar field energy $U_\Phi(\mathbf{x}) \propto (\Delta\Phi(\mathbf{x}))^2$. Furthermore, the structures underlying the image are assumed to be modeled as a mesh of spring-attached point masses in a state of equilibrium with those scalar fields. Although equilibrium assumes that there is an external force field, the shape of the force field is not important. The distribution of the point masses is assumed to change in time, and the total energy change in a time period Δt after time $t = n$ is given by

$$\Delta U_n(\Delta x) = \sum_{\forall X \in g_n} [(\alpha(g_n(x) - g_{n+1}(x+\Delta x)))^2 + (\beta(|\nabla g_n(x)| - |\nabla g_{n+1}(x+\Delta x)|))^2 + (\gamma(\nabla^2 g_n(x) + \nabla^2 g_{n+1}(x+\Delta x)))^2 + \frac{1}{2}\eta \Delta X^T K \Delta X]$$

where α, β, and γ are weights for the contribution of every individual field change, η weighs the gain in the strain energy, $\mathbf{K}$ is the FEM stiffness matrix, and $\Delta\mathbf{X}$ is the FEM node displacement matrix. Analysis of that equation shows that any change in the image fields or in the mesh point distribution increases the system total energy. Therefore, the point correspondence from g_n to g_{n+1} is given by the mesh configuration whose total energy variation is a minimum. Accordingly, the point correspondence is given by

$$\hat{X} = X + \Delta\hat{X}$$

where

$$\Delta\hat{X} = \min_{\Delta X} \Delta U_n(\Delta X).$$

In that notation, $\min_p q$ is the value of p that minimizes q.

While the equations set forth above could conceivably be used to estimate the motion (point correspondence) of every voxel in the image, the number of voxels, which is typically over one million, and the complex nature of the equations make global minimization difficult. To simplify the problem, a coarse FEM mesh is constructed with selected points from the image at step 305. The energy minimization gives the point correspondence of the selected points.

The selection of such points is not trivial. First, for practical purposes, the number of points has to be very small, typically $\cong 10^4$; care must be taken that the selected points describe the whole image motion. Second, region boundaries are important features because boundary tracking is enough for accurate region motion description. Third, at region boundaries, the magnitude of the gradient is high, and the Laplacian is at a zero crossing point, making region boundaries easy features to track. Accordingly, segmented boundary points are selected in the construction of the FEM.

Although the boundary points represent a small subset of the image points, there are still too many boundary points for practical purposes. In order to reduce the number of points, constrained random sampling of the boundary points is used for the point extraction step. The constraint consists of avoiding the selection of a point too close to the points already selected. That constraint allows a more uniform selection of the points across the boundaries. Finally, to reduce the motion estimation error at points internal to each region, a few more points of the image are randomly selected using the same distance constraint. Experimental results show that between 5,000 and 10,000 points are enough to estimate and describe the motion of a typical volumetric image of 256×256×34 voxels. Of the selected points, 75% are arbitrarily chosen as boundary points, while the remaining 25% are interior points. Of course, other percentages can be used where appropriate.

Once a set of points to track is selected, the next step is to construct an FEM mesh for those points at step 307. The mesh constrains the kind of motion allowed by coding the material properties and the interaction properties for each region. The first step is to find, for every nodal point, the neighboring nodal point. Those skilled in the art will appreciate that the operation of finding the neighboring nodal point corresponds to building the Voronoi diagram of the mesh. Its dual, the Delaunay triangulation, represents the best possible tetrahedral finite element for a given nodal configuration. The Voronoi diagram is constructed by a dilation approach. Under that approach, each nodal point in the discrete volume is dilated. Such dilation achieves two purposes. First, it is tested when one dilated point contacts another, so that neighboring points can be identified. Second, every voxel can be associated with a point of the mesh.

Once every point x_i has been associated with a neighboring point x_j, the two points are considered to be attached by a spring having spring constant $k_{i,j}^{l,m}$, where l and m identify the materials. The spring constant is defined by the material interaction properties of the connected points; those material interaction properties are predefined by the user in accordance with known properties of the materials. If the connected points belong to the same region, the spring constant reduces to $k_{i,j}^{l,l}$ and is derived from the elastic properties of the material in the region. If the connected points belong to different regions, the spring constant is derived from the average interaction force between the materials at the boundary.

In theory, the interaction must be defined between any two adjacent regions. In practice, however, it is an acceptable approximation to define the interaction only between major anatomical components in the image and to leave the rest as arbitrary constants. In such an approximation, the error introduced is not significant compared with other errors introduced in the assumptions set forth above.

Spring constants can be assigned automatically, particularly if the region of interest includes tissues or structures whose approximate size and image intensity are known *a priori*, e.g., bone. Segmented image regions matching the *a priori* expectations are assigned to the relatively rigid elastic constants for bone. Soft tissues and growing or shrinking brain lesions are assigned relatively soft elastic constants.

Once the mesh has been set up, the next image in the sequence is input at step 309, and the energy between the two successive images in the sequence is minimized at step 311. The problem of minimizing the energy U can be split into two separate problems: minimizing the energy associated with rigid motion and minimizing that associated with deformable motion. While both energies use the same energy function, they rely on different strategies.

The rigid motion estimation relies on the fact that the contribution of rigid motion to the mesh deformation energy $(\Delta \mathbf{X}^T \mathbf{K} \Delta \mathbf{X})/2$ is very close to zero. The segmentation and the *a priori* knowledge of the anatomy indicate which points belong to a rigid body. If such points are selected for every individual rigid region, the rigid motion energy minimization is accomplished by finding, for each rigid region R_i, the rigid motion rotation $\mathbf{R}_i$ and the translation $\mathbf{T}_i$ that minimize that region's own energy:

$$\Delta X_{rigid} = \min_{\Delta x} U_{rigid} = \sum_{\forall i \in rigid} (\Delta \hat{X} = \min_{\Delta x_i} U_n(\Delta X_i))$$

where $\Delta \mathbf{X}_i = \mathbf{R}_i \cdot \mathbf{X}_i + \mathbf{T}_i \mathbf{X}_i$ and $\Delta \hat{x}_i$ is the optimum displacement matrix for the points that belong to the rigid region R_i. That minimization problem has only six degrees of freedom for each rigid region: three in the rotation matrix and three in the translation matrix. Therefore, the twelve components (nine rotational and three translational) can be found via a six-dimensional steepest-descent technique if the difference between any two images in the sequence is small enough.

Once the rigid motion parameters have been found, the deformational motion is estimated through minimization of the total system energy U. That minimization cannot be simplified as much as the minimization of the rigid energy, and without further considerations, the number of degrees of freedom in a 3D deformable object is three times the number of node points in the entire mesh. The nature of the problem allows the use of a simple gradient descent technique for each node in the mesh. From the potential and kinetic energies, the Lagrangian (or kinetic potential, defined in physics as the kinetic energy minus the potential energy) of the system can be used to derive the Euler-Lagrange equations for every node of the system where the driving local force is just the gradient of the energy field. For every node in the mesh, the local energy is given by

$$U_{X_i,n}(\Delta x) =$$
$$(\alpha(g_n(x_i+\Delta x)-g_{n+1}(x_i)))^2+(\beta(|\nabla g_n(x_i+\Delta x)|-|\nabla g_{n+1}(x_i)|))^2+$$
$$\gamma(\nabla^2 g_n(x_i+\Delta x)+\nabla^2 g_{n+1}(x_i))^2+\frac{1}{2}\eta\sum_{x_j\in G_m(x_i)}(k_{i,j}^{l,m}(x_j-x_i-\Delta x))^2$$

where G_m represents a neighborhood in the Voronoi diagram.

Thus, for every node, there is a problem in three degrees of freedom whose minimization is performed using a simple gradient descent technique that iteratively reduces the local node energy. The local node gradient descent equation is

$$x_i(n+1)=x_i(n)-\nu\Delta U_{(x_i(n),n)}(\Delta x)$$

where the gradient of the mesh energy is analytically computable, the gradient of the field energy is numerically estimated from the image at two different resolutions, x(n+1) is the next node position, and v is a weighting factor for the gradient contribution.

At every step in the minimization, the process for each node takes into account the neighboring nodes' former displacement. The process is repeated until the total energy reaches a local minimum, which for small deformations is close to or equal to the global minimum. The displacement vector thus found represents the estimated motion at the node points.

Once the minimization process just described yields the sampled displacement field ΔX, that displacement field is used to estimate the dense motion field needed to track the segmentation from one image in the sequence to the next (step 313). The dense motion is estimated by weighting the contribution of every neighbor mode in the mesh. A constant velocity model is assumed, and the estimated velocity of a voxel x at a time t is v(x, t) = Δx(t)/Δt. The dense motion field is estimated by

$$v(x,t)=\frac{c(x)}{\Delta t}\sum_{\forall\Delta x_j\in G_m(x_i)}\frac{k^{l,m}\Delta x_j}{|x-x_j|}$$

where

$$c(x) = \left[\sum_{\forall \Delta x_j \in G_m(x_i)} \frac{k^{l,m}}{|x - x_j|} \right]^{-1}$$

$k^{l,m}$ is the spring constant or stiffness between the materials l and m associated with the voxels $\mathbf{x}$ and $\mathbf{x}_j$, Δt is the time interval between successive images in the sequence, $|\mathbf{x} - \mathbf{x}_j|$ is the simple Euclidean distance between the voxels, and the interpolation is performed using the neighbor nodes of the closest node to the voxel $\mathbf{x}$. That interpolation weights the contribution of every neighbor node by its material property $k_{i,j}^{l,m}$; thus, the estimated voxel motion is similar for every homogeneous region, even at the boundary of that region.

Then, at step 315, the next image in the sequence is filled with the segmentation data. That means that the regions determined in one image are carried over into the next image. To do so, the velocity is estimated for every voxel in that next image. That is accomplished by a reverse mapping of the estimated motion, which is given by

$$v(x, t + \Delta t) = \frac{1}{H} \sum_{\forall [x_j + v(x_j, t)] \in S(x)} v(x_j, t)$$

where H is the number of points that fall into the same voxel space $S(\mathbf{x})$ in the next image. That mapping does not fill all the space at time $t+\Delta t$, but a simple interpolation between mapped neighbor voxels can be used to fill out that space. Once the velocity is estimated for every voxel in the next image, the segmentation of that image is simply

$$L(x, t + \Delta t) = L(x - v(x, t + \Delta t)\Delta t, t)$$

where $L(\mathbf{x},t)$ and $L(\mathbf{x},t+\Delta t)$ are the segmentation labels at the voxel $\mathbf{x}$ for the times t and $t+\Delta t$.

At step 317, the segmentation thus developed is adjusted through relaxation labeling, such as that done at steps 211 and 215, and fine adjustments are made to the mesh nodes in the image. Then, the next image is input at step 309, unless it is determined at step 319 that the last image in the sequence has been segmented, in which case the operation ends at step 321.

The operations described above can be implemented in a system such as that shown in the block diagram of Fig. 4. System 400 includes an input device 402 for input of the image data, the database of material properties, and the like. The information input through the input device 402 is received in the workstation 404, which has a storage device 406 such as a hard drive, a processing unit 408 for performing the processing disclosed above to provide the 4D data, and a graphics rendering engine 410 for preparing the 4D data for viewing, e.g., by surface rendering. An output device 412 can include a monitor for viewing the images rendered by the rendering engine 410, a further storage device such as a video recorder for recording the images, or both. Illustrative examples of the workstation 304 and the graphics rendering engine 410 are a Silicon Graphics Indigo workstation and an Irix Explorer 3D graphics engine.

Shape and topology of the identified biomarkers can be quantified by any suitable techniques known in analytical geometry. The preferred method for quantifying shape and topology is with the morphological and topological formulas as defined by the references cited above.

The data are then analyzed over time as the individual is scanned at later intervals. There are two types of presentations of the time trends that are preferred. In one class, successive measurements are overlaid in rapid sequence so as to form a movie. In the complementary representation, a trend plot is drawn giving the higher

order measures as a function of time. For example, the mean and standard deviation (or range) of a quantitative assessment can be plotted for a specific local area, as a function of time.

The accuracy of those measurements and their sensitivity to subtle changes in small substructures are highly dependent on the resolution of the imaging system. Unfortunately, most CT, MRI, and ultrasound systems have poor resolution in the out-of-plane, or "z" axis. While the in-plane resolution of those systems can commonly resolve objects that are just under one millimeter in separation, the out-of-plane (slice thickness) is commonly set at 1.5mm or even greater. For assessing subtle changes and small defects using higher order structural measurements, it is desirable to have better than one millimeter resolution in all three orthogonal axes. That can be accomplished by fusion of a high resolution scan in the orthogonal, or out-of-plane direction, to create a high resolution voxel data set (Peña, J.-T., Totterman, S.M.S., Parker, K.J. "MRI Isotropic Resolution Reconstruction from Two Orthogonal Scans," *SPIE Medical Imaging*, 2001, hereby incorporated by reference in its entirety into the present disclosure). In addition to the assessment of subtle defects in structures, that high-resolution voxel data set enables more accurate measurement of structures that are thin, curved, or tortuous.

In following the response of a person or animal to therapy, or to monitor the progression of disease, it is desirable to accurately and precisely monitor the trends in biomarkers over time. That is difficult to do in conventional practice since repeated scans must be reviewed independently and the biomarkers of interest must be traced or measured manually or semi-manually with each time interval representing a new and tedious process for repeating the measurements. It is highly advantageous to take a 4D approach, such as was defined in the above-cited patent to *Parker et al*, where a

biomarker is identified with statistical reasoning, and the biomarker is tracked from scan to scan over time. That is, the initial segmentation of the biomarker of interest is passed on to the data sets from scans taken at later intervals. A search is done to track the biomarker boundaries from one scan to the next. The accuracy and precision and reproducibility of that approach is superior to that of performing manual or semi-manual measurements on images with no automatic tracking or passing of boundary information from one scan interval to subsequent scans.

The quantitative assessment of the new biomarkers listed above provides an objective measurement of the state of the region of interest, particularly in the progression of neurological diseases. It is also very useful to obtain accurate measurements of those biomarkers over time, particularly to judge the degree of response to a new therapy, or to assess the trends with increasing age. Manual and semi-manual tracings of conventional biomarkers (such as the simple thickness or volume of the cartilage) have a high inherent variability, so as successive scans are traced the variability can hide subtle trends. That means that only gross changes, sometimes over very long time periods, can be verified in conventional methods. The inventors have discovered that by extracting the biomarker using statistical tests, and by treating the biomarker over time as a 4D object, with an automatic passing of boundaries from one time interval to the next, provides a highly accurate and reproducible segmentation from which trends over time can be detected. Thus, the combination of selected biomarkers that themselves capture subtle pathologies, with a 4D approach to increase accuracy and reliability over time, creates sensitivity that has not been previously obtainable.

While a preferred embodiment of the invention has been set forth above, those skilled in the art who have reviewed the present disclosure will readily appreciate that

other embodiments can be realized within the scope of the present invention. For example, any suitable imaging technology can be used. Therefore, the present invention should be construed as limited only by the appended claims.

We claim:

1. A method for assessing a neurological condition of a patient, the method comprising:

(a) taking at least one three-dimensional image of a region of interest of the patient, the region of interest comprising part of the nervous system of the patient;

(b) identifying, in the at least one three-dimensional image, at least one biomarker of the nervous system of the patient;

(c) deriving at least one quantitative measurement of the at least one biomarkers; and

(d) storing an identification of the at least one biomarker and the at least one quantitative measurement in a storage medium.

2. The method of claim 1, wherein step (d) comprises storing the at least one three-dimensional image in the storage medium.

3. The method of claim 1, wherein step (b) comprises statistical segmentation of the at least one three-dimensional image to identify the at least one biomarker.

4. The method of claim 1, wherein the at least one three-dimensional image comprises a plurality of three-dimensional images of the region of interest taken over time.

5. The method of claim 4, wherein step (b) comprises statistical segmentation of a three-dimensional image selected from the plurality of three-dimensional images to identify the at least one biomarker.

6. The method of claim 5, wherein step (b) further comprises motion tracking and estimation to identify the at least one biomarker in the plurality of three-dimensional images in accordance with the at least one biomarker identified in the selected three-dimensional image.

7. The method of claim 6, wherein the plurality of three-dimensional images and the at least one biomarker identified in the plurality of three-dimensional images are used to form a model of the region of interest and the at least one biomarker in three dimensions of space and one dimension of time.

8. The method of claim 7, wherein the biomarker is tracked over time in the model.

9. The method of claim 1, wherein a resolution in all three dimensions of the at least one three-dimensional image is finer than 1 mm.

10. The method of claim 1, wherein the at least one biomarker is selected from the group consisting of:

- a shape, topology, and morphology of brain lesions;
- a shape, topology, and morphology of brain plaques;
- a shape, topology, and morphology of brain ischemia;
- a shape, topology, and morphology of brain tumors;
- a spatial frequency distribution of sulci and gyri;
- a compactness of gray matter and white matter;
- whole brain characteristics;
- gray matter characteristics;
- white matter characteristics;
- cerebral spinal fluid characteristics;
- hippocampus characteristics;
- brain sub-structure characteristics;
- a ratio of cerebral spinal fluid volume to gray matter and white matter volume; and
- a number and volume of brain lesions.

11. The method of claim 1, wherein step (a) is performed through magnetic resonance imaging.

12. A system for assessing a neurological condition of a patient, the system comprising:

(a) an input device for receiving at least one three-dimensional image of a region of interest of the patient, the region of interest comprising part of the nervous system of the patient;

(b) a processor, in communication with the input device, for receiving the at least one three-dimensional image of the region of interest, identifying, in the at least one three-dimensional image, at least one biomarker of the nervous system of the patient and deriving at least one quantitative measurement of the at least one biomarker;

(c) storage, in communication with the processor, for storing an identification of the at least one biomarker and the at least one quantitative measurement; and

(d) an output device for displaying the at least one three-dimensional image, the identification of the at least one biomarker and the at least one quantitative measurement.

13. The system of claim 12, wherein the storage also stores the at least one three-dimensional image.

14. The system of claim 12, wherein the processor identifies the at least one biomarker through statistical segmentation of the at least one three-dimensional image.

15. The system of claim 12, wherein the at least one three-dimensional image comprises a plurality of three-dimensional images of the region of interest taken over time.

16. The system of claim 15, wherein the processor identifies the at least one biomarkers through statistical segmentation of a three-dimensional image selected from the plurality of three-dimensional images.

17. The system of claim 16, wherein the processor uses motion tracking and estimation to identify the at least one biomarker in the plurality of three-dimensional images in accordance with the at least one biomarker identified in the selected three-dimensional image.

18. The system of claim 17, wherein the plurality of three-dimensional images and the at least one biomarker identified in the plurality of three-dimensional images are used to form a model of the region of interest and the at least one biomarker in three dimensions of space and one dimension of time.

19. The system of claim 12, wherein a resolution in all three dimensions of the at least one three-dimensional image is finer than 1 mm.

20. The system of claim 12, wherein the at least one biomarker is selected from the group consisting of:

- a shape, topology, and morphology of brain lesions;
- a shape, topology, and morphology of brain plaques;
- a shape, topology, and morphology of brain ischemia;
- a shape, topology, and morphology of brain tumors;
- a spatial frequency distribution of sulci and gyri;
- a compactness of gray matter and white matter;
- whole brain characteristics;
- gray matter characteristics;
- white matter characteristics;
- cerebral spinal fluid characteristics;

- hippocampus characteristics;
- brain sub-structure characteristics;
- a ratio of cerebral spinal fluid volume to gray matter and white matter volume; and
- a number and volume of brain lesions.

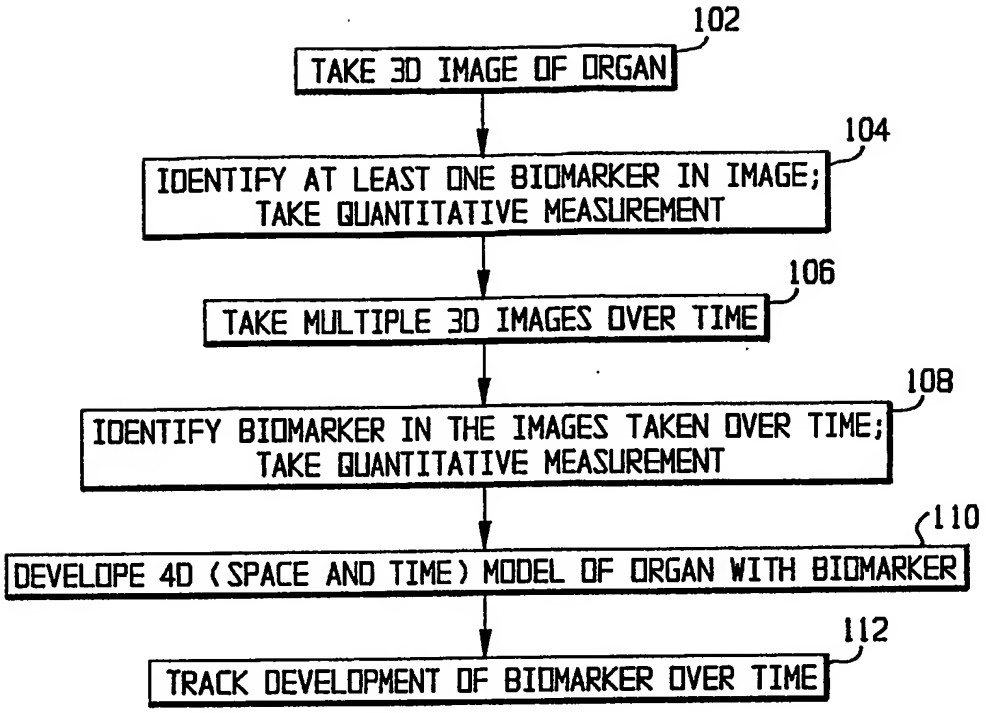
102
TAKE 3D IMAGE OF ORGAN
104
IDENTIFY AT LEAST ONE BIOMARKER IN IMAGE; TAKE QUANTITATIVE MEASUREMENT
106
TAKE MULTIPLE 3D IMAGES OVER TIME
108
IDENTIFY BIOMARKER IN THE IMAGES TAKEN OVER TIME; TAKE QUANTITATIVE MEASUREMENT
110
DEVELOPE 4D (SPACE AND TIME) MODEL OF ORGAN WITH BIOMARKER
112
TRACK DEVELOPMENT OF BIOMARKER OVER TIME

FIG. 1

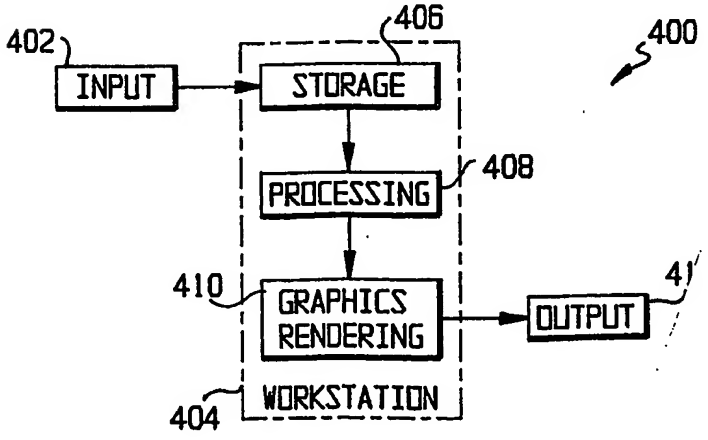
402
INPUT
406
STORAGE
400
PROCESSING
408
410
GRAPHICS RENDERING
OUTPUT
WORKSTATION
404

FIG. 4

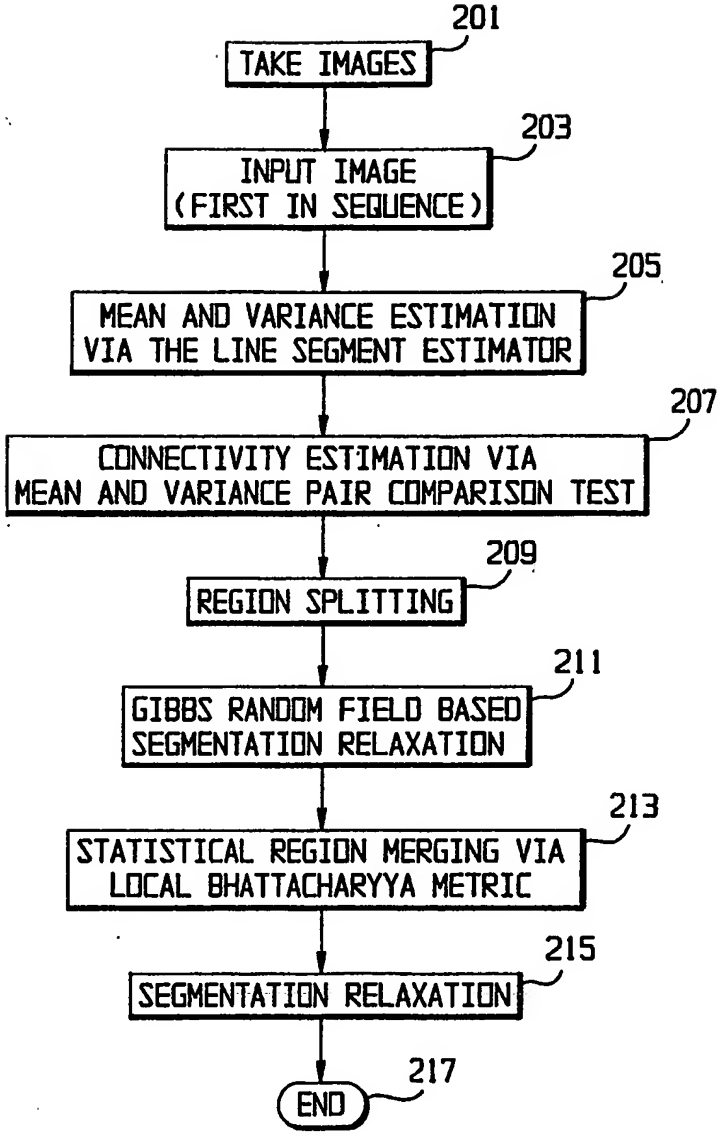
201
TAKE IMAGES
203
INPUT IMAGE (FIRST IN SEQUENCE)
205
MEAN AND VARIANCE ESTIMATION VIA THE LINE SEGMENT ESTIMATOR
207
CONNECTIVITY ESTIMATION VIA MEAN AND VARIANCE PAIR COMPARISON TEST
209
REGION SPLITTING
211
GIBBS RANDOM FIELD BASED SEGMENTATION RELAXATION
213
STATISTICAL REGION MERGING VIA LOCAL BHATTACHARYYA METRIC
215
SEGMENTATION RELAXATION
217
END

FIG. 2

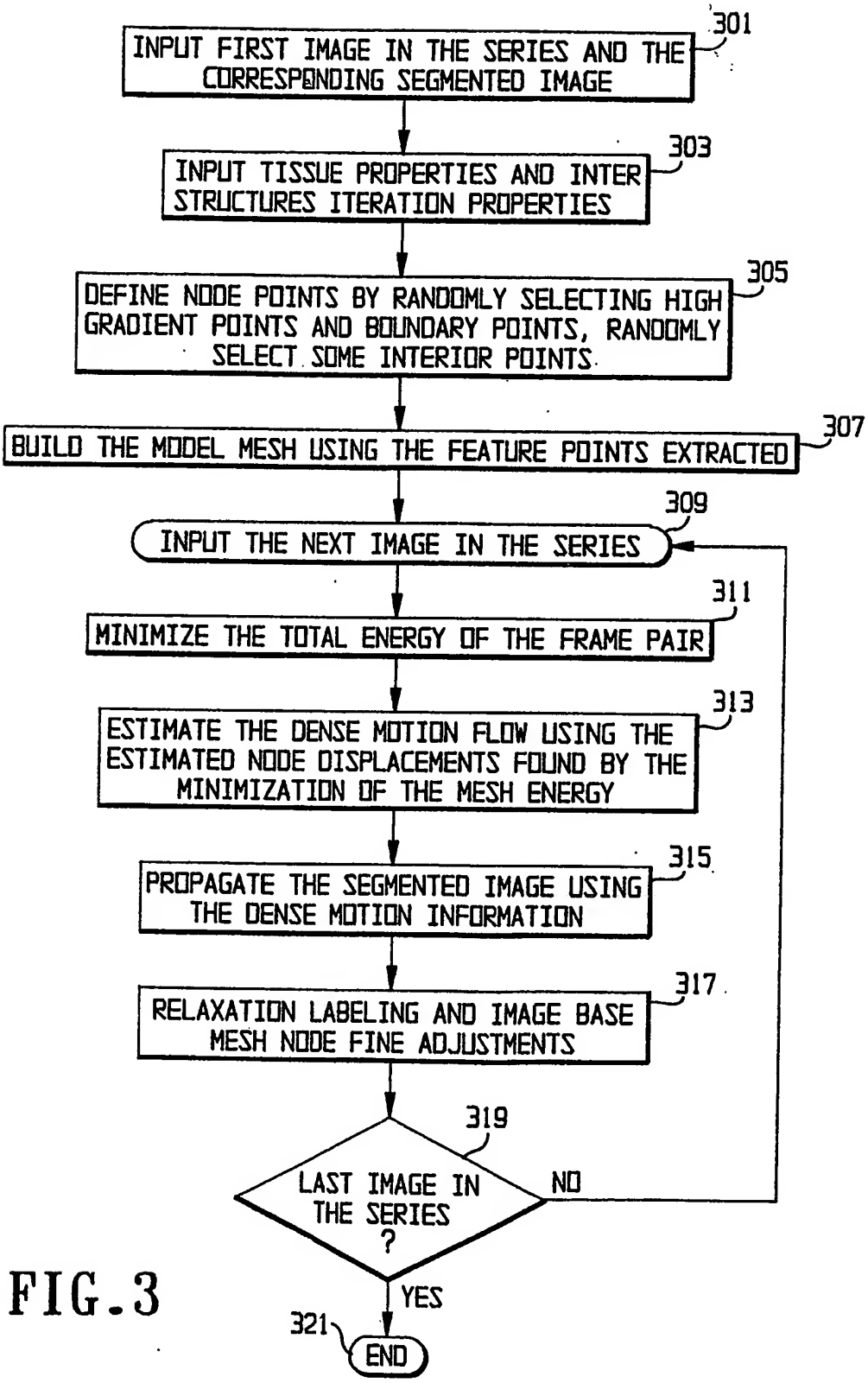
INPUT FIRST IMAGE IN THE SERIES AND THE CORRESPONDING SEGMENTED IMAGE
301
INPUT TISSUE PROPERTIES AND INTER STRUCTURES ITERATION PROPERTIES
303
DEFINE NODE POINTS BY RANDOMLY SELECTING HIGH GRADIENT POINTS AND BOUNDARY POINTS, RANDOMLY SELECT SOME INTERIOR POINTS
305
BUILD THE MODEL MESH USING THE FEATURE POINTS EXTRACTED
307
INPUT THE NEXT IMAGE IN THE SERIES
309
MINIMIZE THE TOTAL ENERGY OF THE FRAME PAIR
311
ESTIMATE THE DENSE MOTION FLOW USING THE ESTIMATED NODE DISPLACEMENTS FOUND BY THE MINIMIZATION OF THE MESH ENERGY
313
PROPAGATE THE SEGMENTED IMAGE USING THE DENSE MOTION INFORMATION
315
RELAXATION LABELING AND IMAGE BASE MESH NODE FINE ADJUSTMENTS
317
LAST IMAGE IN THE SERIES ?
319
NO
YES
END
321

FIG.3

INTERNATIONAL SEARCH REPORT

International application No.
PCT/US02/28070

A. CLASSIFICATION OF SUBJECT MATTER
IPC(7) : G 06K 9/00
US CL : 382/131
According to International Patent Classification (IPC) or to both national classification and IPC

B. FIELDS SEARCHED

Minimum documentation searched (classification system followed by classification symbols)
U.S. : 382/131

Documentation searched other than minimum documentation to the extent that such documents are included in the fields searched

Electronic data base consulted during the international search (name of data base and, where practicable, search terms used)

C. DOCUMENTS CONSIDERED TO BE RELEVANT

Category *	Citation of document, with indication, where appropriate, of the relevant passages	Relevant to claim No.
Y	US 6,112,112 A (GILHUIJS et al.) 29 August 2000 col. 3 lines 15-19; col. 4 lines 21-42 and 33-35; col. 5 lines 1-10; col. 6 lines 60-65; col. 9 lines 38-53; and col. 10 lines 10-20	1-20
Y	US 5,185,809 A (KENNEDY et al.) 09 February 1993 col. 1 lines 62-67; col. 2 lines 4-11, 36-42, and 53-56; col. 3 lines 8-25; col. 4 lines 11-18	1-20
Y	US 6,277,074 B1 (CHSTURVEDI et al.) 21 August 2001 col. 4 lines 16-30	6-8,17, and 18
Y	US 5,785,654 A (IINUMA et al.) 28 July 1998, all.	6-8, 17, and 18
Y,P	US 6,368,331 B1 (FRONT et al.) 09 August 2002 col. 3 lines 44-45	9 and 19
A	US 5,068,788 (GOODENOUGH et al.) 26 November 1991, col. 2 lines 62-65,col. 3 lines 20-40, and col. 6 lines 55-62	1-20

☐ Further documents are listed in the continuation of Box C. ☐ See patent family annex.

* Special categories of cited documents:

"A" document defining the general state of the art which is not considered to be of particular relevance

"E" earlier application or patent published on or after the international filing date

"L" document which may throw doubts on priority claim(s) or which is cited to establish the publication date of another citation or other special reason (as specified)

"O" document referring to an oral disclosure, use, exhibition or other means

"P" document published prior to the international filing date but later than the priority date claimed

"T" later document published after the international filing date or priority date and not in conflict with the application but cited to understand the principle or theory underlying the invention

"X" document of particular relevance; the claimed invention cannot be considered novel or cannot be considered to involve an inventive step when the document is taken alone

"Y" document of particular relevance; the claimed invention cannot be considered to involve an inventive step when the document is combined with one or more other such documents, such combination being obvious to a person skilled in the art

"&" document member of the same patent family

Date of the actual completion of the international search
19 November 2002 (19.11.2002)

Date of mailing of the international search report
17 DEC 2002

Name and mailing address of the ISA/US
Commissioner of Patents and Trademarks
Box PCT
Washington, D.C. 20231
Facsimile No. (703)305-3230

Authorized officer
Amelia Au
Telephone No. 703-305-4700

Form PCT/ISA/210 (second sheet) (July 1998)